Continuous monitoring of elemental mercury employing low-cost multimode diode lasers

2015 Meas. Sci. Technol. 26 085501

(http://iopscience.iop.org/0957-0233/26/8/085501)

IOP Publishing Measurement Science and Technology
Meas. Sci. Technol. **26** (2015) 085501 (7pp) doi:10.1088/0957-0233/26/8/085501

Continuous monitoring of elemental mercury employing low-cost multimode diode lasers

Hongze Lin[1], Xiutao Lou[2], Weijia Zhong[1] and Sailing He[1,3]

[1] Centre for Optical and Electromagnetic Research, Zhejiang Provincial Key Laboratory for Sensing Technologies, Zhejiang University (ZJU), Hangzhou, 310058, People's Republic of China
[2] Department of Physics, Harbin Institute of Technology, Harbin 150001, People's Republic of China
[3] ZJU-SCNU Joint Research Center of Photonics, Centre for Optical and Electromagnetic Research, South China Academy of Advanced Optoelectronics, South China Normal University (SCNU), 510006 Guangzhou, People's Republic of China

E-mail: louxiutao@gmail.com

Received 23 November 2014, revised 6 April 2015
Accepted for publication 8 April 2015
Published 2 July 2015

Abstract

A continuous monitoring system for elemental mercury detection utilizing low-cost multimode diode lasers is demonstrated. Ultraviolet light with a central wavelength at 253.7 nm is generated through sum-frequency generation. Correlation spectroscopy is employed to trace the signals of the target gas by using a reference gas cell. Algorithms including automatic peak searching and multiple-linear-regression are employed to retrieve the mercury concentration, and long term measurements are performed. For a path length of 1 m, a sensitivity of $0.12\,\mu g\,m^{-3}$ (13.4 ppt) is achieved for a 60 s integration time, and the linear dynamic range is about $0 \sim 60\,\mu g\,m^{-3}$. Experimental results show that the present system has great potential for industrial applications.

Keywords: mercury, continuous monitoring, diode laser, absorption spectroscopy

(Some figures may appear in colour only in the online journal)

1. Introduction

Mercury is the only liquid metal that is highly volatile at room temperature. Its toxic effects include damage to the brain, kidneys and lungs [1], which have raised academic and public concern for many years. The predominant anthropogenic emitters of mercury include mines, municipal waste incineration [2], fossil fuel combustion [3], chlor-alkali plants [4] and non-ferrous metal smelting processes. Other potential sources include disposed mercury-based batteries, fluorescent light tubes, pesticides, clinical thermometers, etc. The emitted mercury enters the food chain primarily through atmospheric deposition followed by bioaccumulation in fish, while consumption of contaminated fish is the primary pathway for human exposure to mercury [5]. Typically, mercury exists in three states: particulate-bound, elemental and oxidized mercury [6]. Current commercial continuous emission monitors (CEMs) for mercury can directly detect elemental mercury concentration. For detection of total mercury concentration, oxidized mercury is always converted into the elemental state by using conversion units based on wet chemistry, thermal cracking or catalysts. Therefore, the elemental mercury measurement is essential for mercury detection.

Various methods for mercury sensing have been reported, most of which are based on optical methods. Cold vapor atomic absorption spectroscopy (CVAAS) [7, 8] and cold vapor atomic fluorescence spectroscopy (CVAFS) [9, 10] are two typical techniques widely deployed. However, the necessity of pretreating the sampled gas consumes excessive amounts of time. Cavity ring down-laser absorption spectroscopy (CRLAS) offers the potential for monitoring mercury at parts per trillion (ppt) levels, but the existence of SO_2 with a concentration greater than 10 ppm may cause interference problems [11, 12]. Zeeman absorption spectroscopy can reach

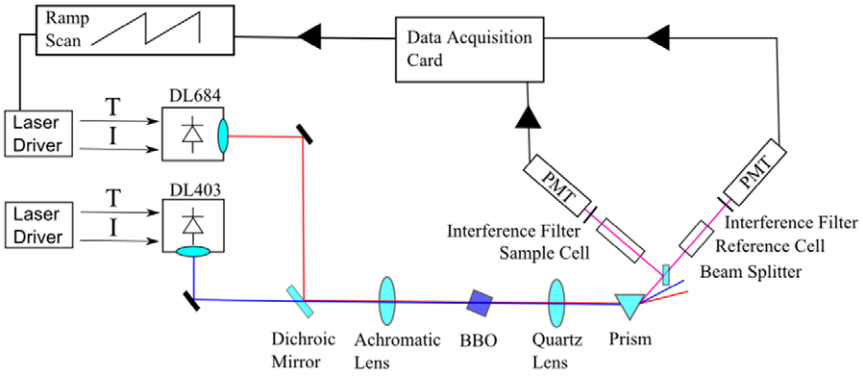

Figure 1. Diagram of the continuous mercury monitoring system.

a detection limit of 2 ng m^{-3} with an average time of 1 s [13, 14], but the lifespan of a mercury lamp is relatively short (around 2000 h). Differential optical absorption spectroscopy (DOAS) [15, 16], as well as light detection and ranging (Lidar) [4, 17] techniques, can detect mercury several kilometers away, but careful calibrations are needed. The laser-induced breakdown spectroscopy (LIBS) technique can also be used to measure mercury concentration [18, 19]; however, the use of a Nd:YAG laser requires careful operation in order to ensure sufficient accuracy.

Mercury measurement by diode lasers (DLs) was proposed and demonstrated for the first time by Alnis *et al* [20]. They used two commercial single-mode visible DLs with central wavelengths at 404 and 688 nm to generate 253.7 nm ultra violet (UV) light. Other DL pairs, e.g. 375 and 784 nm, also have been employed for mercury detection [3]. Despite the good accuracy and detection limit, single-mode lasers are often expensive, and the mode-hop-free tuning range is relatively small. In our previous work, a multimode violet DL and an FP type quasi-single-mode red DL were employed as light sources to generate a multimode ultraviolet laser for detection of mercury concentration [21]. It is commonly known that the lifetime of multimode DLs is much longer than that of mercury lamps, and their price is much lower than that of single mode DLs. The drawback is that the laser emission spectrum may change from time-to-time due to the mode competition. To stay up-to-date with the spectrum change, correlation spectroscopy [22] was employed by using a reference channel with a known mercury concentration. The previous mercury sensing system has several limitations. Firstly, the measurement sensitivity was mainly limited by shot noise due to the weak UV light detected, as lasers with low output power and optical filters with low transmissions were employed. Secondly, the absorption signals were randomly selected without any optimization, hence the optimal performance of the system was not achieved. Thirdly, only a qualitative analysis was performed because of the inaccurate concentration calibration and calculation algorithm. Fourthly, some of the system components used were too large to build a miniaturized system, e.g. two photomultiplier tubes (PMTs) with large volumes.

In this paper, in order to solve the above limiting problems, the mercury monitoring system is rebuilt by utilizing two multi-mode DLs with larger output powers, optical filters with higher transmissions, and PMT modules with smaller volumes and higher UV light sensitivity. A new concentration retrieval method is developed using a derivative method, automatic peak searching algorithm and multiple-linear-regression approach. Quantitative mercury measurements are performed employing sample cells of various thicknesses. Long-term monitoring is performed to check the robustness and stability of the system. Finally, experiments of mercury volatilization are carried out, the measurement results of which may be of interest to research fields related to volatilization.

2. Experimental setup

The experimental setup of the continuous mercury monitoring system is illustrated in figure 1. The violet (Sony, SLD3134, 20 mW) and red (Roithner laser technic, QL68J6S-A, 50 mW) laser beams are guided together by a dichroic mirror, and focused into a Beta-Barium-Borate (BBO) crystal to generate UV light. The output light, collimated by quartz lenses, is dispersed by a fused silica prism. The UV light is then separated by a 50/50 beam splitter into two channels, one passing through a reference cell and the other through a sample cell. Both cells contain mercury inside, with the concentration of mercury vapor determined by the cell temperature [23]. Both the reference and the sample laser beams are detected by photomultiplier modules (Hamamatsu H10493-12) with a 254 nm interference filter mounted on each head. The peak transmittance of the interference filter is about 12% with a full-width-half-maximum (FWHM) of 10 nm, so that the background light is blocked out. The PMT module integrates a PMT, a high voltage power supply, and a low noise amplifier all in one tube, making it a preferable choice for minimizing the system. The PMT output voltage signals are acquired by a data acquisition (DAQ) card (PCI-6120, National Instruments) and transferred to a computer for real-time data analysis by LabVIEW-based programs.

In general, the emission wavelengths of both DLs redshift along with a rise in operating current and temperature. By tuning the temperatures and the currents of both DLs, the wavelength of the generated UV light can be adjusted. Because the output wavelength of the violet DL is locked at 403 nm by stabilizing the temperature and the input current, a scheme of a current scan of the red laser can be performed.

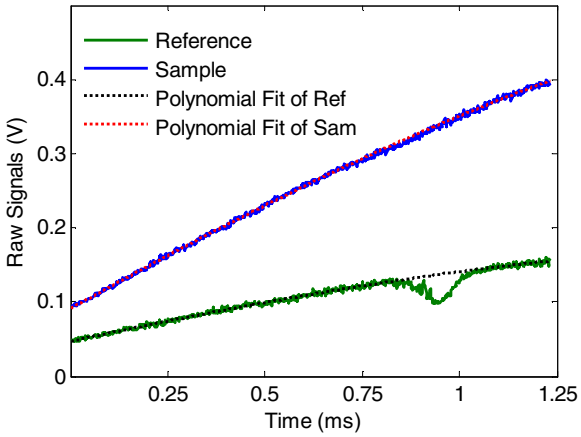

Figure 2. Typical raw signals of the reference channel (a 3.10 mm mercury cell) and sample channel (no gas cell).

The on-resonance signals of mercury are obtained by ramp-sweeping the current of the red laser from 60 to 100 mA at a repetition rate of 800 Hz. The sampling rate of the DAQ card is 800 000 samples s^{-1}, so each spectrum is composed of 1000 points, which can offer an adequate resolution. Each measurement signal is an average of 1000 successive signal sweeps, throughout a period of 1.25 s.

3. Measurement and analysis

3.1. Raw signal

Figure 2 shows typical recorded raw signals of the reference channel (a 3.10 mm mercury cell) and sample channel (no gas cell). The spectrum encompasses an average of 1000 sweeps. An absorption signal can be observed on the reference line, with an absorption amplitude of ~26%. The tuning range is more than 100 GHz, providing an adequate off-resonant baseline to fit the original light intensity. The sample channel here is not used for baseline corrections, but simply to check that there are no obvious intensity fluctuations due to mode hops and that the baseline can be fitted well by a third order polynomial.

3.2. Signal preprocessing

In order to guarantee the measurement accuracy, raw signals are preprocessed before the concentration retrieval. The absorption baseline is corrected automatically and the absorption spectrum is extracted with little influence from the variation in light intensity and absorption. To correct the baseline, the absorption peak position is first searched, and then the beginning and end points of the absorption are determined by a derivative method.

The raw signal is first smoothed by the Savitzky–Golay (SG) filter, a smoothing method that can maintain the shape and width of the absorption signal. A second order polynomial is chosen for obtaining smoother results [24]. The smoothed spectrum is then followed by a standard normal variate (SNV) [25] procedure to remove variation in the slope due to light intensity changes. The SNV transformed spectrum (x_{SNV}) is

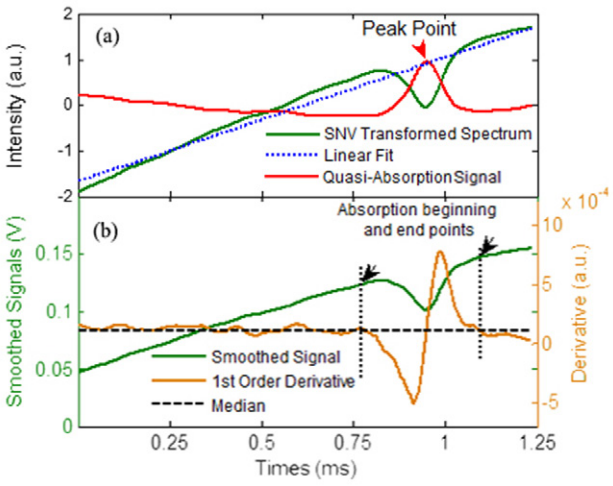

Figure 3. (a) Automatic locating procedure for absorption peak. The green, blue and red lines are the SNV transformed spectrum, its linear fit and quasi-absorption signal, respectively. (b) Automatic searching procedure of the beginning and end points of the absorption signal. The green, orange and black lines are the smoothed raw signal, its first order derivative, and the median of the derivative, respectively. The dotted line indicates the beginning and end positions of the absorption signal.

$$x_{SNV} = \frac{x - \bar{x}}{s} \tag{1}$$

where $\bar{x}$ represents the mean value of the spectrum and s represents the standard deviation. Next, the x_{SNV} is subtracted by its linear fit, resulting in a quasi-absorption signal (figure 3(a)). This time, a peak searching algorithm is applied to find peak points that are larger than 0.1, a criterion set to separate the absorption peaks from the influence of light intensity fluctuation or optical noise.

After locating the absorption peak, the first order derivative of the reference channel is utilized to find the beginning and end points of the absorption signal. Because the raw signal increases linearly as a whole, the median of the first order derivative can be considered to be the slope of the whole ramp. The points before and after the absorption peak whose derivative values equal the median are considered to be the beginning and end absorption points (figure 3(b)).

It is of great importance to find the beginning and end absorption points correctly and automatically, especially for a multimode laser system. Known as a drawback, the wavelength of the output of a multimode laser will fluctuate due to even a small change in operating temperature, resulting in a shift in position and change in shape of the absorption signal. Figures 4(a) and (b) show two particular absorption signal shapes. In figure 4(a), there exist two absorption peaks in the scanning range, while in figure 4(b) the two absorption peaks overlap. The existence of the two peaks is due to mode-hop, where the wavelength of DLs may 'jump' back when the laser current increases, as described in [21]. The presented processing method can successfully locate the beginning and end points of the absorption signals.

According to the beginning and end points of the absorption, the baseline can be corrected by applying a third-order

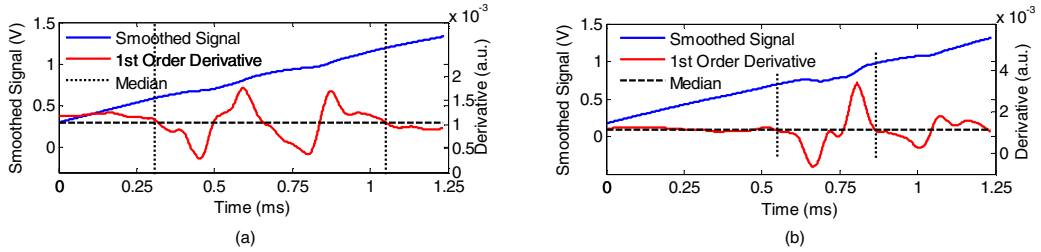

Figure 4. (a) Dual-peak absorption signals. (b) Overlapped absorption signals.

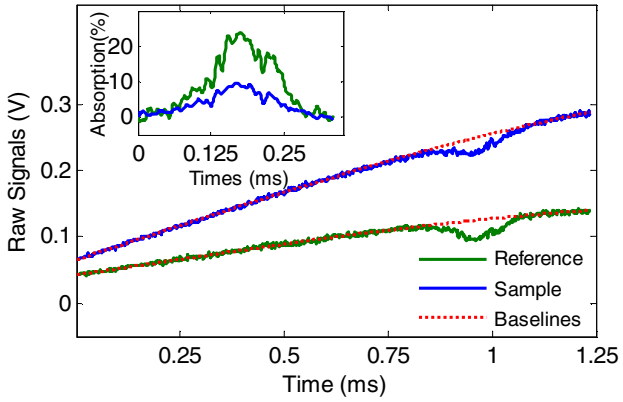

Figure 5. Sample and reference signals with their baseline obtained by polynomial fitting. The inset is the normalized absorption signals of the reference channel (green line) and sample channel (blue line).

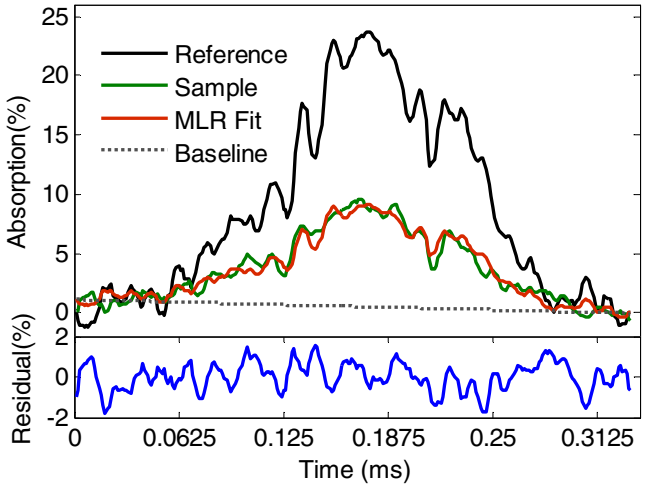

Figure 6. MLR-fit results of the sample absorption signal. The fitted background baseline is also shown.

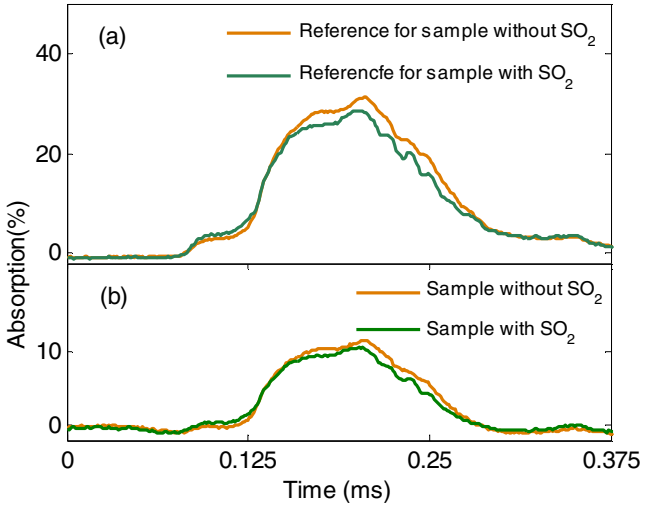

Figure 7. (a) Reference absorption signals of mercury vapor (3.10 mm). (b) Sample absorption signals of mercury vapor with and without interference of SO_2 (1000 ppm, 10 cm).

polynomial interpolation over the full transmission region on both sides of the absorption signal, which corresponds to the initial laser intensity without mercury absorption (the red dotted line in figure 2). The absorption amplitudes can be retrieved, as shown in figure 5, from the raw signals and the fitted initial intensities.

3.3. Sample concentration determination

As shown in figure 5, the absorption signal trembles due to the unstable light intensities of the longitudinal modes of DLs. These highly-correlated signals provide special fingerprints that can be utilized by correlation spectroscopy to distinguish the absorption of mercury from interfering gases, e.g. SO_2 and NO_2. The ratio between the reference absorption spectrum of the known concentration and the sample absorption spectrum of the unknown concentration is determined by a multiple-linear-regression (MLR) approach [26, 27]. In the MLR approach, the background structure is accommodated by an offset and a linear term. A quadratic term is not included because the absorption signal sometimes resembles a parabola shape, and the quadratic term may induce a distorted background fit and consequently affect the final measurement accuracy. The sample absorption signal is fitted by a combination of a term corresponding to the reference spectrum and the two baseline terms mentioned above:

$$S = A_1 R + A_2 + A_3 X \tag{2}$$

where S and R represent the sample and the reference spectrum, respectively. A_i represents the best-fit parameters, and X represents the x numbers in the fitting window. Figure 6 shows the MLR-fit results of the sample absorption signal. The normalized residuals are less than 2%, indicating that the sample spectrum and the MLR-fit spectrum correlate well. The concentration of the sample cell is then determined by A_1:

$$C_{\mathrm{Sam}} = A_1 \cdot \frac{L_{\mathrm{Ref}}}{L_{\mathrm{Sam}}} \cdot C_{\mathrm{Ref}} \tag{3}$$

where L_{Ref} and L_{Sam} represent the lengths of the reference cell and the sample cell, respectively. C_{Sam} and C_{Ref} represent the

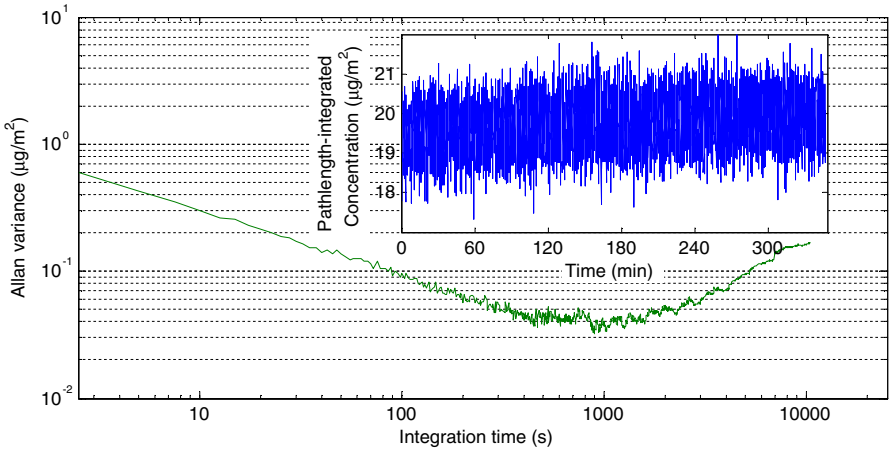

Figure 8. Allan variance plot for 6 h of succesive measurements.

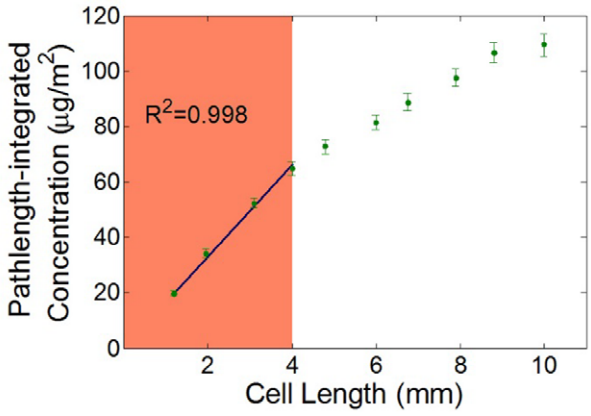

Figure 9. Measured sample cell length versus the calculated pathlength-integrated concentrations.

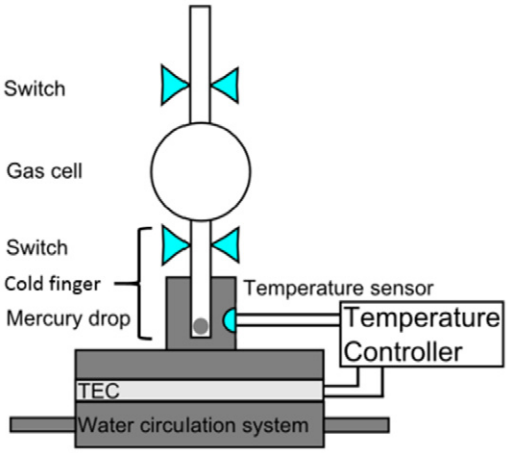

Figure 10. Mercury concentration controlling system.

corresponding concentrations of mercury in the two cells. C_{Ref} is calculated according to the mercury temperature.

4. Performance characterization

The main gas that interferes with mercury from stock emission is SO_2 due to its overlapping resonance region with mercury. Luckily, its absorption spectrum is relatively 'flat' around 253.7 nm, acting as a broadband attenuator in the scanning region. Thus, the absorption signals of mercury can be extracted from the sample signals with little interference from SO_2. In order to inspect the system selectivity, experiments are done by adding a 10 cm gas cell filled with 1000 ppm SO_2 to the sample channel along with the mercury cell. Figure 7 shows the absorption signals (averaging over 625 s) for both the reference and sample cell under conditions with and without SO_2. The discrepancy is mainly due to the fluctuations in the wavelength and intensity of the generated UV light. Since the discrepancy exhibits identical impacts on the sample and reference signal, there is little effect on the concentration retrieval.

The sensitivity performance of the proposed mercury monitoring system is evaluated by performing an Allan variance analysis [28, 29] on 6 h of continuous measurements. The reference cell is 1.95 mm thick, and the sample cell is 1.20 mm thick. The room temperature is measured to be 22 ± 0.2 °C, with a corresponding concentration of 16.6 ± 0.3 mg m^{-3}. Because of the relatively stable conditions during the experiments, the mercury vapor concentrations in both cells are assumed to be constant and equal, so the pathlength-integrated concentration should be around 19.9 μg m^{-2}. During the 6 h measurements, about 8300 successive measurements are performed, each taking approximately 2.5 s (2000 times averaged). The Allan variance plot (figure 8) indicates a sensitivity of 0.12 μg m^{-2} (concentration unit per integrated path length, which equals 13.4 ppt-m), i.e. 0.12 μg m^{-3} for a 1 m path length with an average time of 60 s. The variance minimum occurs at an integration time of 15.6 min, reaching an optimum sensitivity of 0.03 μg m^{-2}, where the white noise becomes dominated by additional drift noise.

The linearity performance of the system is also evaluated. Figure 9 shows a scatter plot of the measured sample cell lengths versus the calculated pathlength-integrated concentrations with the cell length in the range of 1–10 mm. A 3.00 mm mercury cell is used as the reference cell. High linearity (R^2 = 0.998) in the low absorption region (cell length from 1 to 4 mm) can be observed, indicating a linear dynamic range of 0 ~ 60 μg m^{-2}. In the high absorption region, the system

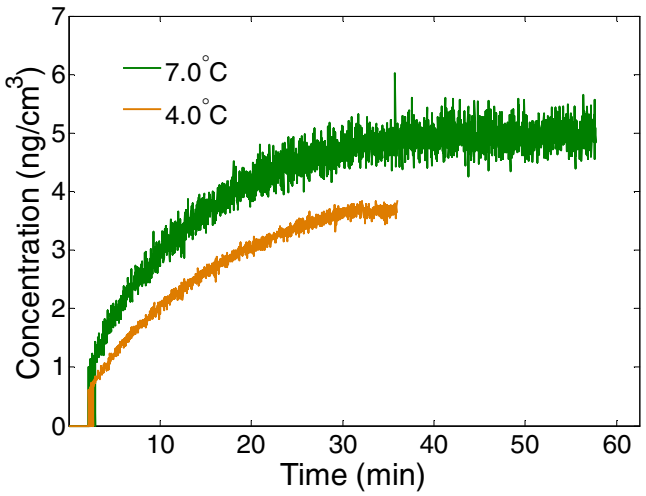

Figure 11. The volatilizing process of mercury over 60 min.

response is nonlinear, and thus a further calibration process is required to obtain accurate measurement results.

In order to evaluate the feasibility of the system for continuous monitoring of industrial mercury emissions, the mercury vapor volatilization process is monitored. A sample cell with a thickness of 10.1 mm is used. The sample cell, as depicted in figure 10, has a cold finger with a mercury drop, as well as an outlet for exhaling. The experiment is carried out by switching off the down switch (so that the liquid mercury is isolated from the gas cell), pumping out all the gases, filling the cell with clean air, and then closing the upper switch and opening the down switch. The reference cell is under room temperature (~20 °C), and the cold finger is cooled and stabilized to 4 and 7 °C respectively by dipping it into a groove attached to a Thermoelectric Cooler (TEC). The concentrations are 3.50 $\mu g\,m^{-3}$ for 4 °C, and 4.59 $\mu g\,m^{-3}$ for 7 °C. Heat produced by the TEC is removed by a water circulation system, and continuous measurements are carried out. The measurement results of the volatilizing process are shown in figure 11. As expected, the mercury concentration increases faster at the beginning, and then slows down to a balanced level. The sudden jump in the first few seconds is caused by the quick diffusion of the mercury vapor stored below the switch, after which the concentration expands by vaporization of the mercury drop. Some interesting phenomena have also been observed: the higher the temperature is set, the quicker the mercury becomes volatile, and also the longer time it takes for the vapor to saturate, which may help to further understand the process of mercury volatilization.

5. Conclusions

A continuous monitoring system of elemental mercury by using low-cost multimode DLs has been demonstrated. An algorithm based on SNV, peak searching and the derivative method is developed to automatically locate the absorption signal and extract the absorption spectrum. To retrieve the sample concentration, a multiple-linear-regression approach is employed. With an average time of 60 s, a typical sensitivity of 0.12 $\mu g\,m^{-2}$ is achieved. The coefficient of linear regression R^2 = 0.998 indicates a good linearity between the retrieved pathlength-integrated concentrations and the cell lengths under low absorption conditions. The present system is promising for on-site monitoring of mercury in industrial fields.

Acknowledgments

This work was partially supported by the Science and Technology Department of Zhejiang Province (2010R50007), the National Natural Science Foundation of China (91233208 and 61008027), a Guangdong Innovative Research Team Program (Grant 201001D0104799318) and the Postdoctoral Scientific Research Developmental Fund of Heilongjiang Province (LBH-Q14069).

References

[1] Clifton J 2007 Mercury exposure and public health *Pediatr. Clin. North Am.* **54** 237–69
[2] Kilgroe J D 1996 Control of dioxin, furan, and mercury emissions from municipal waste combustors *J. Hazard. Mater.* **47** 163–94
[3] Anderson T N, Magnuson J K and Lucht R P 2007 Diode-laser-based sensor for ultraviolet absorption measurements of atomic mercury *Appl. Phys.* B **87** 341–53
[4] Edner H, Faris G W, Sunesson A and Svanberg S 1989 Atmospheric atomic mercury monitoring using differential absorption lidar techniques *Appl. Opt.* **28** 921–30
[5] Stein E D, Cohen Y and Winer A M 1996 Environmental distribution and transformation of mercury compounds *Crit. Rev. Environ. Sci. Technol.* **26** 1–43
[6] Magnuson J K, Anderson T N, Lucht R P, Vijayasarathy U A, Oh H, Annamalai K and Caton J A 2008 Application of a diode-laser-based ultraviolet absorption sensor for *in situ* measurements of atomic mercury in coal-combustion exhaust *Energy Fuels* **22** 3029–36
[7] Hight S C and Cheng J 2005 Determination of total mercury in seafood by cold vapor-atomic absorption spectroscopy (CVAAS) after microwave decomposition *Food Chem.* **91** 557–70
[8] Balarama Krishna M V, Ranjit M, Karunasagar D and Arunachalam J 2005 A rapid ultrasound-assisted thiourea extraction method for the determination of inorganic and methyl mercury in biological and environmental samples by CVAAS *Talanta* **67** 70–80
[9] Geng W, Nakajima T, Takanashi H and Ohki A 2008 Determination of mercury in ash and soil samples by oxygen flask combustion method–cold vapor atomic fluorescence spectrometry (CVAFS) *J. Hazard. Mater.* **154** 325–30
[10] da Silva M J, Paim A P S, Pimentel M F, Cervera M L and de la Guardia M 2010 Determination of mercury in rice by cold vapor atomic fluorescence spectrometry after microwave-assisted digestion *Anal. Chim. Acta* **667** 43–8
[11] Spuler S, Linne M, Sappey A and Snyder S 2000 Development of a cavity ringdown laser absorption spectrometer for detection of trace levels of mercury *Appl. Opt.* **39** 2480–6
[12] Berden G, Peeters R and Meijer G 2000 Cavity ring-down spectroscopy experimental schemes and applications *Int. Rev. Phys. Chem.* **19** 565–607

[13] Sholupov S, Pogarev S, Ryzhov V, Mashyanov N and Stroganov A 2004 Zeeman atomic absorption spectrometer RA-915+ for direct determination of mercury in air and complex matrix samples *Fuel Process. Technol.* **85** 473–85
[14] Hadeishi T, Church D A, McLaughlin R D, Zak B D, Nakamura M and Chang B 1975 Mercury monitor for ambient air *Science* **187** 348–9
[15] Edner H, Sunesson A, Svanberg S, Uneus L and Wallin S 1986 Differential optical absorption spectroscopy system used for atmospheric mercury monitoring *Appl. Opt.* **25** 403–9
[16] Thoma E D, Secrest C, Hall E S, Lee J D, Shores R C, Modrak M, Hashmonay R and Norwood P 2009 Measurement of total site mercury emissions from a chlor-alkali plant using ultraviolet differential optical absorption spectroscopy and cell room roof-vent monitoring *Atmos. Environ.* **43** 753–7
[17] Guan Z G, Lundin P, Mei L, Somesfalean G and Svanberg S 2010 Vertical lidar sounding of atomic mercury and nitric oxide in a major Chinese city *Appl. Phys.* B **101** 465–70
[18] Lazzari C, De Rosa M, Rastelli S, Ciucci A, Palleschi V and Salvetti A 1994 Detection of mercury in air by time-resolved laser-induced breakdown spectroscopy technique *Laser Part. Beams* **12** 525–30
[19] Fang X and Ahmad S R 2012 Detection of mercury in water by laser-induced breakdown spectroscopy with sample pre-concentration *Appl. Phys.* B **106** 453–6
[20] Alnis J, Gustafsson U, Somesfalean G and Svanberg S 2000 Sum-frequency generation with a blue diode laser for mercury spectroscopy at 254 nm *Appl. Phys. Lett.* **76** 1234–6
[21] Lou X T, Somesfalean G, Svanberg S, Zhang Z G and Wu S H 2012 Detection of elemental mercury by multimode diode laser correlation spectroscopy *Opt. Express* **20** 4927–38
[22] Lou X T, Somesfalean G, Chen B, Zhang Y G, Wang H S, Zhang Z G, Wu S H and Qin Y K 2010 Simultaneous detection of multiple-gas species by correlation spectroscopy using a multimode diode laser *Opt. Lett.* **35** 1749–51
[23] Huber M L, Laesecke A and Friend D G 2006 Correlation for the vapor pressure of mercury *Ind. Eng. Chem. Res.* **45** 7351–61
[24] Chen J, Jönsson P, Tamura M, Gu Z H, Matsushiba B and Eklundh L 2004 A simple method for reconstructing a high-quality NDVI time-series data set based on the Savitzky–Golay filter *Remote Sensing Environ.* **91** 332–44
[25] Barnes R J, Dhanoa M S and Lister S J 1989 Standard normal variate transformation and de-trending of near-infrared diffuse reflectance spectra *Appl. Spectrosc.* **43** 772–7
[26] Roller C, Fried A, Walega J, Weibring P and Tittel F 2006 Advances in hardware, system diagnostics software, and acquisition procedures for high performance airborne tunable diode laser measurements of formaldehyde *Appl. Phys.* B **82** 247–64
[27] Gagliardi G, Castrillo A, Iannone R Q, Kerstel E R T and Gianfrani L 2003 High-precision determination of the $13CO_2/12CO_2$ isotope ratio using a portable 2.008 μm diode-laser spectrometer *Appl. Phys.* B **77** 119–24
[28] Werle P W, Mazzinghi P, D'Amato F, De Rosa M, Maurer K and Slemr F 2004 Signal processing and calibration procedures for *in situ* diode-laser absorption spectroscopy *Spectrochim. Acta A Mol. Biomol. Spectrosc.* **60** 1685–705
[29] Werle P, Mucke R and Slemr F 1993 The limits of signal averaging in atmospheric trace-gas monitoring by tunable diode-laser absorption spectroscopy (TDLAS) *Appl. Phys.* B **57.2** 131–9